

UniICL: Systematizing Unified Multimodal In-context Learning through a Capability-Oriented Taxonomy

Yicheng Xu¹, Jiangning Zhang^{1,*†}, Zhucun Xue¹, Teng Hu², Ran Yi², Xiaobin Hu³, Yong Liu^{1,†}, Dacheng Tao⁴

¹Zhejiang University, ²Shanghai Jiaotong University, ³National University of Singapore, ⁴Nanyang Technological University

*Equal contributions, †Corresponding authors

In-context Learning enables training-free adaptation via demonstrations but remains highly sensitive to example selection and formatting. In unified multimodal models spanning understanding and generation, this sensitivity is exacerbated by cross-modal interference and varying cognitive demands. Consequently, In-context Learning efficacy is often non-monotonic and highly task-dependent. To diagnose these behaviors, we introduce a six-level capability-oriented taxonomy that categorizes the functional role of demonstrations from basic perception to high-order discernment. Guided by this cognitive framework, we construct UniICL-760K, a large-scale corpus featuring curated 8-shot In-context Learning episodes across 15 subtasks, alongside UniICL-Bench for rigorous, controlled evaluation. As an architectural intervention to stabilize few-shot adaptation, we propose the Context-Adaptive Prototype Modulator, a lightweight, plug-and-play module. Evaluations on UniICL-Bench show that our approach yields highly competitive unified results, outperforming larger-parameter multimodal large language model baselines on most understanding In-context Learning tasks. Data and code will be available soon at <https://github.com/xuyicheng-zju/UniICL>.

Date: March 27, 2026

Correspondence: 186368@zju.edu.cn

Code: <https://github.com/xuyicheng-zju/UniICL>

Data: <https://huggingface.co/datasets/xuyicheng-zju/UniICL-760K>



1 Introduction

In-context Learning (ICL) drives training-free generalization [4], enabling systems to perform novel tasks via few-shot demonstrations. This paradigm is increasingly applied to multimodal systems [1, 18, 20, 21] and image synthesis [8, 15, 22]. As architectures evolve toward unified models jointly supporting understanding and generation, integrating robust ICL across disparate tasks within a shared interface becomes exceptionally difficult. The dense interleaving of text and visual tokens frequently introduces cross-modal interference. This makes unified ICL highly sensitive to demonstration selection and modality balance [5, 26, 29], complicating practical deployment.

Existing research often approaches multimodal ICL through task- or modality-specific lenses (Fig. 1, left). Prevailing multimodal datasets and benchmarks [19, 24, 47] focus predominantly on zero-shot evaluation. The few existing ICL datasets remain modality asymmetric, heavily favoring visual question answering over generative tasks [17], and lack a systematic cognitive structure [51]. This fragmentation mixes distinct cognitive demands, treating demonstrations interchangeably as low-level perceptual anchors or abstract analogical scaffolds [1, 20, 22]. Consequently, the specific scaling behaviors of ICL under varying cognitive loads remain obscured, and the phenomenon of *non-monotonic shot scaling* (Fig. 1, top-left) is largely unexplored. Adding demonstrations can degrade perception-dominant tasks due to visual distraction while simultaneously improving complex inductive tasks by reinforcing structural patterns.

Diagnosing these failure modes requires a capability-oriented perspective. As our fundamental contribution,

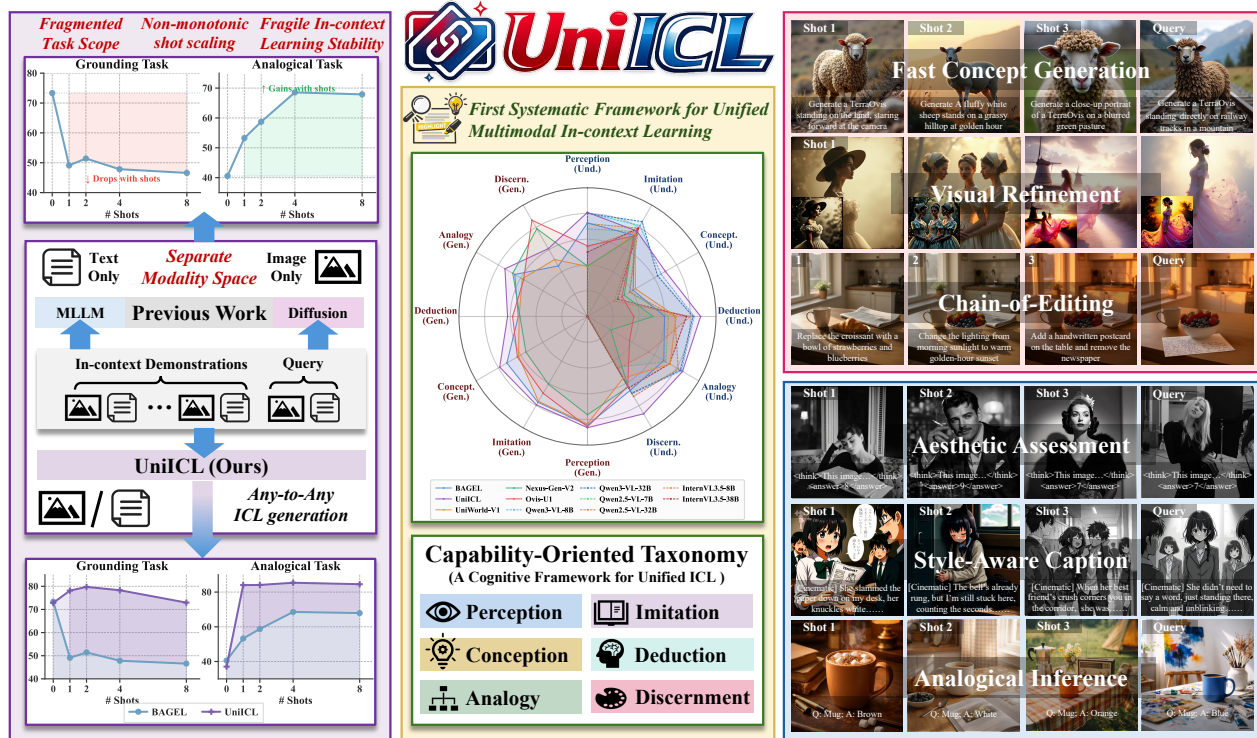


Figure 1 Left: Previous fragmented paradigms isolate modalities and tasks, often suffering from *non-monotonic shot scaling*. Our UniICL mitigates this issue to achieve consistent gains. **Middle:** Our six-level capability-oriented taxonomy and a radar chart across understanding and generation tasks. **Right:** ICL examples from UniICL-760K.

we introduce a six-level taxonomy (Fig. 1, center) inspired by neurocognitive development [6, 9, 11]. It systematically structures ICL tasks by the functional role of demonstrations: perception, imitation, conception, deduction, analogy, and discernment. Guided by this taxonomy, we construct UniICL-760K, the first large-scale dataset specifically targeting unified multimodal ICL, comprising over 766,000 curated episodes across 15 subtasks (partially illustrated in Fig. 1, right). From this collection, we derive UniICL-Bench, serving as the first cognitively structured testbed to systematically evaluate multi-dimensional ICL capabilities and stability in up to 8-shot settings.

While our structured dataset establishes the foundation for unified multimodal In-context Learning, standard self-attention mechanisms remain susceptible to cross-modal noise in dense contexts. As an auxiliary architectural enhancement to maximize ICL benefits, we propose the Context-Adaptive Prototype Modulator (CAPM). This lightweight, plug-and-play module explicitly disentangles demonstration encoding and dynamically adjusts context routing to stabilize few-shot adaptation, ensuring models can translate additional demonstrations into consistent gains. In summary, our core contributions are threefold:

- We introduce a six-level capability-oriented taxonomy that standardizes multimodal ICL evaluation based on the cognitive role of demonstrations, exposing non-monotonic scaling behaviors in unified models.
- As our primary contribution, we present UniICL-760K and UniICL-Bench, providing the first comprehensive, cognitively structured training corpus and rigorous evaluation suite for unified visual understanding and generative ICL.
- We propose CAPM, an auxiliary context-adaptive modulation module. Evaluations on UniICL-Bench show it significantly enhances ICL performance, achieving highly competitive unified results and outperforming larger-parameter MLLMs on most understanding ICL tasks.

2 Related Work

2.1 Multimodal In-Context Learning

In-context learning emerged as a foundational capability in large language models such as GPT-3 [4], enabling training-free adaptation through mechanisms including implicit gradient descent [40], Bayesian inference [46], and induction heads [28]. Extending this capability to the visual domain, systems such as Flamingo [1], BLIP-2 [20], and IDEFICS [16] use interleaved image-text demonstrations as grounding cues for perception-centric tasks like visual question answering and image captioning. Parallel research in visual synthesis, including Visualcloze [22] and CoDi-2 [36], frames in-context conditioning as spatial editing and style transfer. These lines of research approach in-context learning through task-specific perspectives, optimizing for either text-output perception or pixel-level manipulation in isolation. To address this fragmentation, our Capability-Oriented Taxonomy organizes context-dependent demands across six levels within a unified evaluation framework that covers both understanding and generation.

2.2 Datasets and Benchmarks for Multimodal ICL

The development of multimodal datasets initially focused on training and evaluating zero-shot capabilities. While instruction-tuning collections in NLP [25, 44] established standardized evaluation protocols, multimodal benchmarks such as MMBench [24], MMMU [47], and SEED-Bench [19] extended this evaluation to vision-language reasoning. Existing datasets for multimodal in-context learning generally separate understanding from generation. They are often modality-asymmetric, favoring visual question answering over generative tasks, and lack a unified cognitive structure by blending low-level perception with complex deduction. This structural deficiency obscures the specific scaling behaviors of in-context learning under varying cognitive loads. To address these gaps, we propose UniICL-760K as the first large-scale dataset for unified understanding and generation guided by a systematic taxonomy. From this collection, we derive UniICL-Bench, serving as the first cognitively structured benchmark to systematically diagnose unified multimodal in-context learning and its stability.

2.3 Unified Multimodal Foundation Models

Unified multimodal models integrate understanding and generation within a single autoregressive backbone. Systems such as GILL [15], DreamLLM [8], Chameleon [38], and the Emu series [34, 35, 43] achieve interleaved multimodal input and output by aligning visual tokens with discrete text vocabularies. Recent models, including BAGEL [7], UniWorld-V1 [23], Nexus-Gen-V2 [48], and Ovis-U1 [41], advance these capabilities while retaining similar architectural foundations. The paradigm of unified multimodal in-context learning aims to achieve broad generalization across diverse tasks using a single model. Unifying these processes introduces specific challenges compared to fragmented approaches. Models face inherent optimization tensions, such as modality competition and the alignment tax caused by heterogeneous token spaces, frequently resulting in unstable few-shot in-context learning behaviors. To mitigate these issues and improve both the efficiency and stability of in-context learning, we introduce the CAPM module.

3 Methodology: Dataset, Benchmark, and Model

3.1 Formulation of Unified Multimodal In-context Learning

Unified Multimodal In-context Learning (Uni-ICL) adapts foundation models to diverse understanding and generation tasks without parameter updates. Beyond architectural unification, it consolidates multimodal demands into a single cohesive prompting framework. We formalize this as a universal conditional prediction problem, where an ICL episode comprises a k -shot context $\mathcal{D} = \{d_i\}_{i=1}^k$ and a target query (x^*, q^*) . Each demonstration is a triplet $d_i = (x_i, q_i, y_i)$: visual input x_i (or \emptyset for text-only), textual instruction q_i , and ground-truth output y_i . Operating over a shared text-image space \mathcal{Y} , the model predicts $y^* \in \mathcal{Y}$ conditioned on the context:

$$y^* \sim p_\theta(\cdot \mid \mathcal{D}, x^*, q^*).$$

This interface naturally supports mixed-modality episodes, determining the output modality via q^* . However, unified adaptation introduces significant challenges: *highly variable task formats and dense text-image interleaving frequently trigger severe cross-modal interference*. Consequently, models exhibit high sensitivity to demonstration selection, causing unstable, non-monotonic scaling. Resolving this requires a capability-oriented framework to diagnose failure modes alongside robust algorithmic interventions for stabilization.

3.2 Curating UniICL-760K Dataset

We introduce **UniICL-760K**, the first large-scale dataset specifically designed for unified multimodal In-context Learning across visual understanding and generation. It contains 766,868 carefully constructed ICL episodes, each paired with a curated 8-shot demonstration context. Rather than fragmenting tasks by isolated application goals, UniICL-760K organizes understanding and generation within a six-level capability-oriented taxonomy, instantiating 15 corresponding subtasks to measure ICL capabilities across all dimensions. To scale this taxonomy-guided suite, we build an automated data curation pipeline combining dense annotation, generative augmentation, task-aligned demonstration retrieval, and strict quality control. In the final training assets, the annotation branch contributes 202,750 high-quality scene-centric samples after multi-stage validation, while the synthetic branch contributes 353,826 filtered generation-side assets that are reused across multiple tasks. [Table 1](#) summarizes the task-level training pools that are ultimately assembled from these assets. Due to the high cost of constructing expert-level editing trajectories, the *Chain-of-Editing* subtask is excluded from the training corpus, retained solely in our benchmark to evaluate generative generalization. Overall, UniICL-760K serves as a scalable training resource for unified multimodal ICL, while the independently curated UniICL-Bench enables systematic evaluation.

3.2.1 Taxonomy-Guided ICL Task Instantiation.

Demonstrations in an ICL episode serve qualitatively different roles depending on the underlying task. To systematically categorize these functional roles, we introduce a **six-level capability-oriented taxonomy** inspired by the neurocognitive progression from shallow perceptual analysis to deep semantic reasoning [6, 9, 11]. *This taxonomy ensures our dataset and benchmark span comprehensive cognitive dimensions rather than fragmented task-specific optimization.*

- **Perception.** At this foundational level, context serves as an explicit perceptual anchor. The model must selectively attend to targeted visual evidence defined by demonstrations, resisting irrelevant distractors or hallucinated priors. We evaluate this fine-grained attentional allocation and spatial localization through *Visual Grounding*, *Attribute Recognition*, and *Image Manipulation*.
- **Imitation.** Moving beyond passive perception, this level evaluates active observational learning. Demonstrations act as instructors, requiring the model to internalize and reproduce specific structural, stylistic, or logical schemas. We instantiate this capability through *Style-Aware Caption*, *Scene Reasoning*, and *Instructional Generation*.
- **Conception.** This level assesses the core fast-mapping capability of robust ICL: rapidly binding novel linguistic symbols to unseen visual concepts. Context introduces counterfactual or out-of-distribution concepts, demanding that the model temporarily adopt definitions established within the episode. We map this cognitive demand to *Fast Concept Mapping* and *Fast Concept Generation*.
- **Deduction.** This level demands extracting causal or temporal sequences across multiple demonstrations. Rather than isolated mappings, context establishes progressive multi-step coherence rules that the model must deduce to resolve the target query. We measure this capacity through *World-Aware Planning* and *Chain-of-Editing*.
- **Analogy.** This category evaluates abstract generalization, requiring the transfer of hidden transformation rules across diverse surface forms (e.g., varying objects or layouts). Given uninstructed demonstrations sharing an underlying intent, the model must autonomously extract the implicit rule. We assess this through *Analogical Inference* and *Analogical Editing*, applying derived rules to novel visual domains.
- **Discernment.** At our highest cognitive level, this category evaluates value judgment. Context conveys human-aligned criteria for beauty, authenticity and creation rather than deterministic rules. We assess

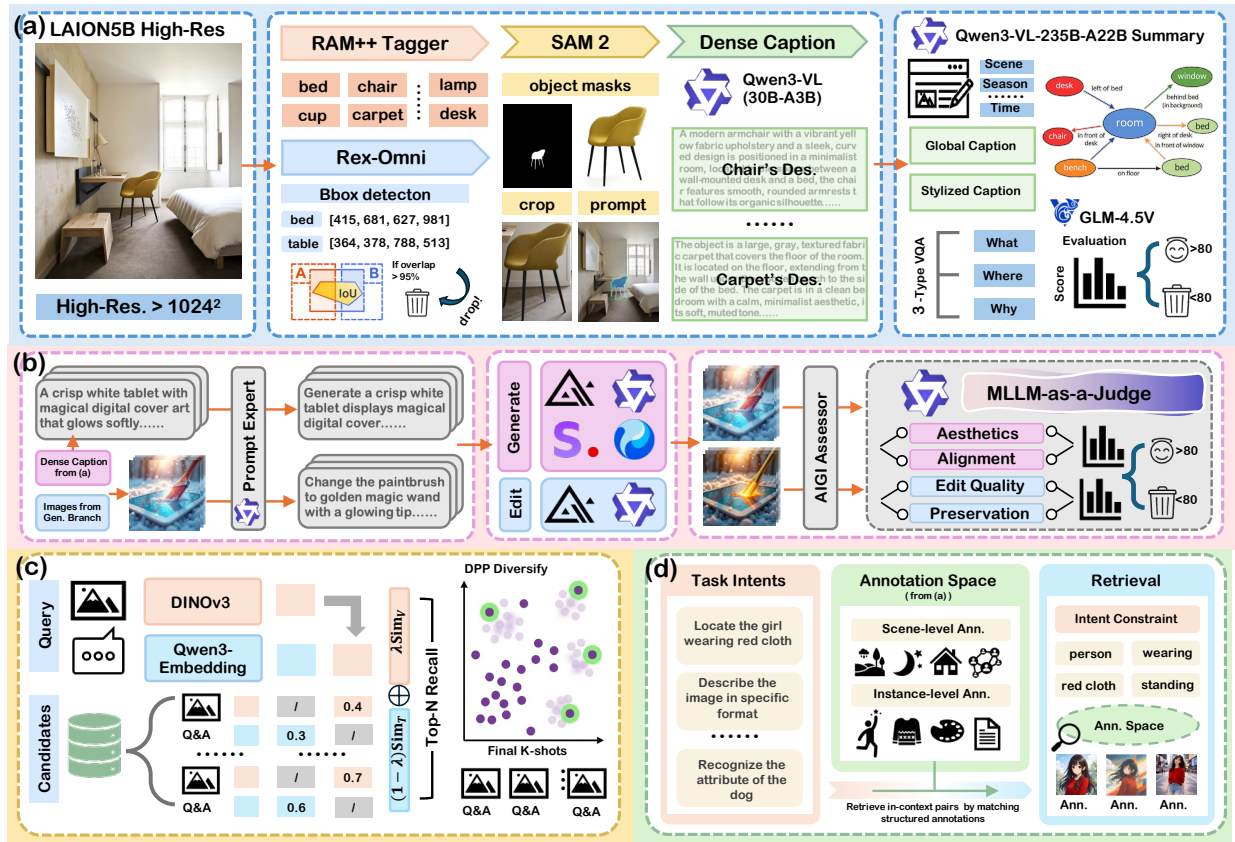


Figure 2 UniICL-760K curation pipeline that includes four processes: **(a)** Cascaded dense annotation for visual knowledge repository construction, **(b)** Generative synthesis and strict quality filtering, **(c)** Multi-modal feature fusion and DPP sampling for continuous semantic retrieval, and **(d)** Intent-driven retrieval from the structured annotation space.

this capability through *Aesthetic Assessment*, *Forgery Detection*, and *Visual Refinement*. To prevent score mimicking, demonstrations include explicit Chain-of-Thought (CoT).

3.2.2 UniICL Curation Pipeline.

Constructing multimodal ICL datasets is inherently costly, requiring rigorous query-demonstration pairing. While prior works [1, 2] rely on basic visual similarity for filtering, this severely limits task coverage. Many ICL tasks require complex structural alignment or abstract rule extraction beyond shared global visual semantics. To curate a large-scale dataset spanning diverse task demands and reflecting our cognitive taxonomy, we design a highly scalable data curation pipeline as shown in Fig. 2.

(1) Automatic Data Asset Construction. We build a highly structured semantic repository via two complementary approaches. **(a) Cascaded Dense Annotation.** To extract fine-grained semantics, we curate a high-resolution LAION-5B [32] subset via a cascaded pipeline. We isolate candidate objects using open-vocabulary tagging (RAM++ [50]) and precise localization (Rex-Omni [14]). Next, SAM 2 [31] performs instance segmentation, generating high-fidelity masks and dual-view representations. We then use Qwen3-VL-30B-A3B-Instruct [3] to generate instance-level dense captions and attributes. Based on these annotations, Qwen3-VL-235B-A22B-Instruct [3] generates comprehensive scene-level summaries (global attributes, stylized captions, scene graphs, and VQA pairs). Finally, GLM-4.5V [13] filters potential hallucinations, reducing the 750k raw-image source to 283,838 validated scene annotations before the final quality threshold, from which 202,750 high-quality samples are retained for training. **(b) Cascaded Generative Synthesis.** To synthesize high-quality images for generative ICL tasks, we expand our dataset using advanced generative and editing expert models (Fig. 3-d). We employ Qwen3-VL-8B-Instruct [3] as a unified prompt expert. For text-to-image

synthesis, it translates Fig. 2-(a) captions into detailed generation prompts, while generating context-aware instructions for image-to-image editing pairs. All outputs are rigorously filtered via dedicated assessment models (Q-Align [45], HPSv3 [27]) and an MLLM-as-a-Judge to retain high-fidelity data, yielding a reusable synthetic asset pool of 353,826 images spanning instruction-following generation, editing, refinement, and concept construction. Concretely, this retained pool comprises 99,455 instruction-following images, 81,202 edited images, 97,683 degraded-clean refinement pairs, and 11,050 concept-oriented synthetic images.

(2) Task-Aligned Demonstration Retrieval. Effective k -shot episodes require retrieving contextual demonstrations aligned with the multimodal query intent $q = (x_q, y_q)$. We adopt a dual-pathway retrieval strategy accommodating varying task abstractions. **(c) Multi-modal Feature Fusion Retrieval.** For tasks relying on semantic alignment, we compute a fused cross-modal similarity between the query q and candidate demonstrations $d = (x_d, y_d)$. Using DINOv3 [33] (E_v) and Qwen3-Embedding [49] (E_t), the fusion score $\mathcal{S}(q, d)$ is defined as:

$$\mathcal{S}(q, d) = \lambda \frac{E_v(x_q) \cdot E_v(x_d)}{\|E_v(x_q)\| \|E_v(x_d)\|} + (1 - \lambda) \frac{E_t(y_q) \cdot E_t(y_d)}{\|E_t(y_q)\| \|E_t(y_d)\|}, \quad (1)$$

where $\lambda=0.5$ balances modality preference. To ensure relevance and diversity, we frame context selection as a Determinantal Point Process (DPP) [37]. For top- N candidates, we construct a positive semi-definite L-ensemble kernel $\mathbf{L}_{ij} = q_i q_j \cdot \phi_i^\top \phi_j$ with $q_i = \exp(\beta \cdot s_i)$, $\beta=8$, where ϕ_i is the ℓ_2 -normalized DINOv3 visual feature of shot d_i and s_i is its multimodal relevance score. This factorizes as $\mathbf{L} = \mathbf{B}\mathbf{B}^\top$ with $\mathbf{B}_i = q_i \phi_i$. The optimal subset is obtained via greedy Cholesky maximization of $\det(\mathbf{L}_Y)$, selecting at each step the candidate with maximum residual norm after projecting out already-selected directions. **(d) Intent-Driven Retrieval from Annotation Space.** Certain implicit inductive tasks resist continuous visual representation. For instance, tasks requiring precise coordinates (e.g., a woman wearing red) are poorly captured by global semantics. Here, we formalize the query intent as a Boolean conceptual rule R . In this example, the logical conjunction is $R = (\text{category} = \text{woman}) \wedge (\text{color} = \text{red}) \wedge (\text{coord} \in \Omega_{\text{target}})$, where Ω_{target} defines the target region. Bypassing the latent space, we evaluate this logic directly against the fine-grained metadata \mathcal{M}_j associated with each candidate demonstration d_j . The context subset is retrieved via exact logical satisfaction:

$$\mathcal{D}_{\text{target}} = \{d_j \in \mathcal{D} \mid \mathcal{M}_j \models R\}, \quad (2)$$

where \models denotes metadata satisfying the Boolean rule R . This ensures the retrieved context strictly adheres to targeted constraints.

The branch-level quality statistics are shown explicitly in Fig. 4. On the annotation side, the final threshold keeps 202,750 samples, with annotation accuracy already concentrated at a high range and scene diversity and object richness acting as the tighter bottlenecks. On the synthetic side, HPSv3 retains 99,455 high-fidelity instruction-following images, while subsequent filtering yields 81,202 edited images and 97,683 refinement pairs with meaningful quality gaps. While Fig. 4 focuses on source-side filtering, Tab. 1 reports the task-level episode pools used in training.

3.2.3 UniICL-Bench Construction and Evaluation

For systematic evaluation, we construct **UniICL-Bench**, a rigorously vetted testbed comprising 1,250 episodes distributed across all six cognitive dimensions. As outlined in Tab. 2, unlike existing benchmarks skewed heavily toward VQA [24, 47] or isolated generation [10], UniICL-Bench provides unified cross-modality assessment within a shared cognitive framework. Its role is intentionally different from that of the training corpus: UniICL-760K supplies large-scale supervision through 202,750 validated scene annotations and 353,826 synthetic assets, whereas UniICL-Bench is kept compact, balanced, and diagnostic.

The benchmark is organized around the same six-level taxonomy as the training set, allowing us to compare understanding and generation under a single capability-oriented view rather than as disconnected task families. As summarized in Tab. 3, the suite spans 15 subtasks, covers both discriminative and generative settings, and preserves free-form response formats instead of collapsing evaluation into multiple-choice templates. This matters because many of our target behaviors, such as concept formation, analogical transfer, or visual refinement, are poorly characterized by categorical answer spaces.

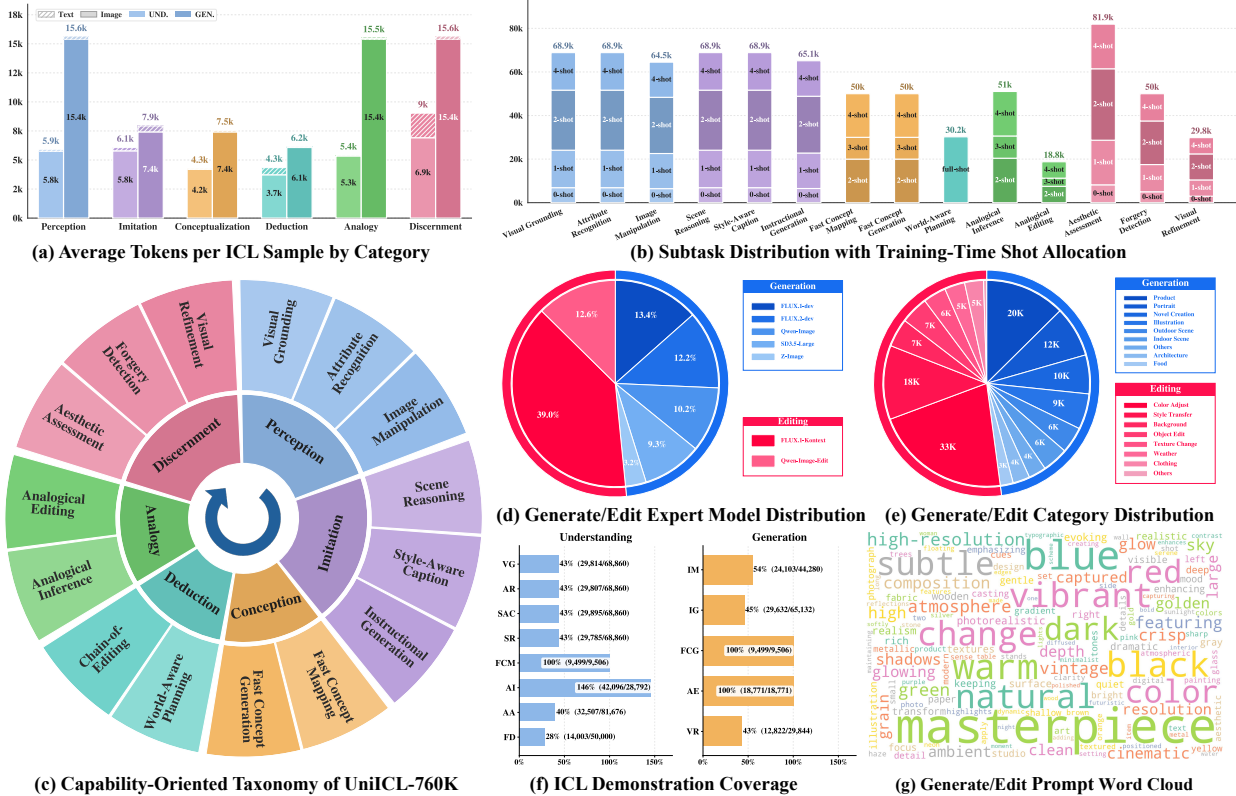


Figure 3 Statistical distributions of our UniICL-760K from multiple perspectives. After filtering, the final training assets combine 202,750 validated scene-centric samples from the annotation branch and 353,826 quality-controlled synthetic assets from the generative branch. The latter break down into 99,455 instruction-following images, 81,202 edited images, 97,683 refinement pairs, and 11,050 concept-oriented synthetic images.

Beyond static accuracy, UniICL-Bench is designed to expose how models use demonstrations. Each task supports controlled shot scaling, and the benchmark further includes dedicated context perturbations to measure robustness under noisy, mismatched, or reordered examples. This makes few-shot stability a first-class evaluation target rather than an afterthought, which distinguishes our benchmark from prior multimodal evaluation suites [53]. To preserve ICL contextual alignment, we avoid multiple-choice reformulations and evaluate all tasks via free-form generation. Deterministic subtasks use standard objective metrics such as accuracy, mIoU, and SRCC/PLCC. For semantically open-ended understanding and generation tasks, we combine specialized neural scorers with an MLLM-as-a-Judge protocol, since single overlap-based metrics are often unreliable for assessing concept transfer, scene reasoning, or instruction-following generation. In particular, we use HPSv3 [27] for instruction-following generation, Q-Align [45] for quality-aware refinement, and MLLM-Judge for tasks whose outputs are valid up to semantic equivalence rather than exact lexical match. For abstract and counterfactual visual generation, where CLIP-Score [12] often fails, this hybrid protocol provides a more faithful view of output quality [52]. The full task-to-metric mapping is summarized in Tab. 3.

3.3 CAPM for Multimodal UniICL Application

We introduce the Context-Adaptive Prototype Modulator (CAPM) in Fig. 5, a lightweight plug-and-play module that converts raw demonstrations into disentangled dynamic representations and injects them into the backbone through a four-stage pipeline.

(a) Decoupled Demonstration Encoding. Standard attention conflates user inputs and assistant responses. To enforce structural disentanglement, we introduce segment-masked cross-attention. Shared backbone embeddings $X_i \in \mathbb{R}^{L_i \times d_b}$ are projected to d_p , and $Y_i = \text{CrossAttn}(Q, X_i W_{in}; M_i)$ is applied with learnable

Table 1 Task-aligned training data overview before benchmark purity filtering. Chain-of-Editing is benchmark-only and is therefore excluded.

Taxonomy	Sub-task	#Samples	Image Source	Episode Assembly
Perception	Visual Grounding	68,860	LAION-HR	Feature-Based
	Attribute Recognition	68,860	LAION-HR	Feature-Based
	Image Manipulation	64,494	Synthesis	Feature-Based
Imitation	Style-Aware Caption	68,860	LAION-HR	Feature-Based
	Scene Reasoning	68,860	LAION-HR	Feature-Based
	Instructional Generation	65,132	Synthesis	Feature-Based
Conception	Fast Concept Mapping	50,000	Synthesis	Intent-Based
	Fast Concept Generation	50,000	Synthesis	Intent-Based
Deduction	World-Aware Planning	30,220	World-Aware Planning	Intent-Based
Analogy	Analogical Inference	51,030	LAION-HR	Intent-Based
	Analogical Editing	18,771	Synthesis	Intent-Based
Discernment	Aesthetic Assessment	81,937	AVA	Feature-Based
	Forgery Detection	50,000	AIGI-Holmes	Feature-Based
	Visual Refinement	29,844	Synthesis	Feature-Based

Table 2 Comparison with open-source multimodal benchmarks. Our proposed UniICL-Bench boasts distinct advantages across various key dimensions.

Benchmark	Scale	Year	Task Coverage		Evaluation Metrics			ICL-Centric Eval.		
			Und.	Gen.	Trad.	Expert	MLLM	0-8 Shot	Taxonomy	Stability
MMBench [24]	3217	2023	✓		✓		✓			
MMMU [47]	11550	2024	✓		✓					
SEED-Bench [19]	19242	2023	✓		✓	✓				
GenEval [10]	553	2023		✓		✓				
VL-ICL-Bench [53]	1760	2024	✓	✓	✓		✓	✓		
UniICL-Bench (Ours)	1250	2026	✓	✓	✓	✓	✓	✓	✓	✓

queries $Q = [q_{in}, q_{out}, q_1, \dots, q_K]$. The segment mask M_i constrains q_{in} and q_{out} to attend exclusively to the user input and assistant response, while the remaining K probes attend to the full sequence. This yields $[c_{in}^{(i)}, c_{out}^{(i)}, C^{(i)}]$, separating the instruction anchor, response anchor, and generic context slots $C^{(i)} = [c_1^{(i)}, \dots, c_K^{(i)}]$.

(b) Low-Rank Transformation and Interaction. To abstract the transformation induced by the demonstration, we derive a discrete token $\hat{z}^{(i)}$. We first pool the generic context slots into a global token $g^{(i)} = \text{Mean}(\text{RMSNORM}(C^{(i)}))$. To capture transition dynamics, we compute the differential ($\Delta^{(i)} = c_{out}^{(i)} - c_{in}^{(i)}$) and interactive ($\Pi^{(i)} = c_{in}^{(i)} \odot c_{out}^{(i)}$) features between anchors. These are concatenated with the original anchors to form a relation descriptor $\phi^{(i)}$, which predicts dynamic modulation coefficients $u^{(i)}, v^{(i)}, \alpha^{(i)}$ for a predefined rank r :

$$\phi^{(i)} = \text{LN}\left(\text{Concat}[c_{in}^{(i)}; c_{out}^{(i)}; \Delta^{(i)}; \Pi^{(i)}]\right), \quad [u^{(i)}, v^{(i)}, \alpha^{(i)}] = \mathcal{H}_{\text{coef}}(\phi^{(i)}). \quad (3)$$

To avoid computing a full $d_p \times d_p$ operator matrix, we maintain shared global bases $U_{\text{base}}, V_{\text{base}} \in \mathbb{R}^{r \times d_p}$. The final $z^{(i)}$ is yielded by modulating $g^{(i)}$ via these dynamic coefficients:

$$z^{(i)} = g^{(i)} + \eta \sum_{k=1}^r \alpha_k^{(i)} \cdot (U_{\text{base},k} \odot u_k^{(i)}) \cdot \langle V_{\text{base},k} \odot v_k^{(i)}, g^{(i)} \rangle. \quad (4)$$

To model inter-demonstration relationships, we stack tokens as $\hat{Z} = [\hat{z}^{(1)}, \dots, \hat{z}^{(N)}]$ and pass them through a self-attention block.

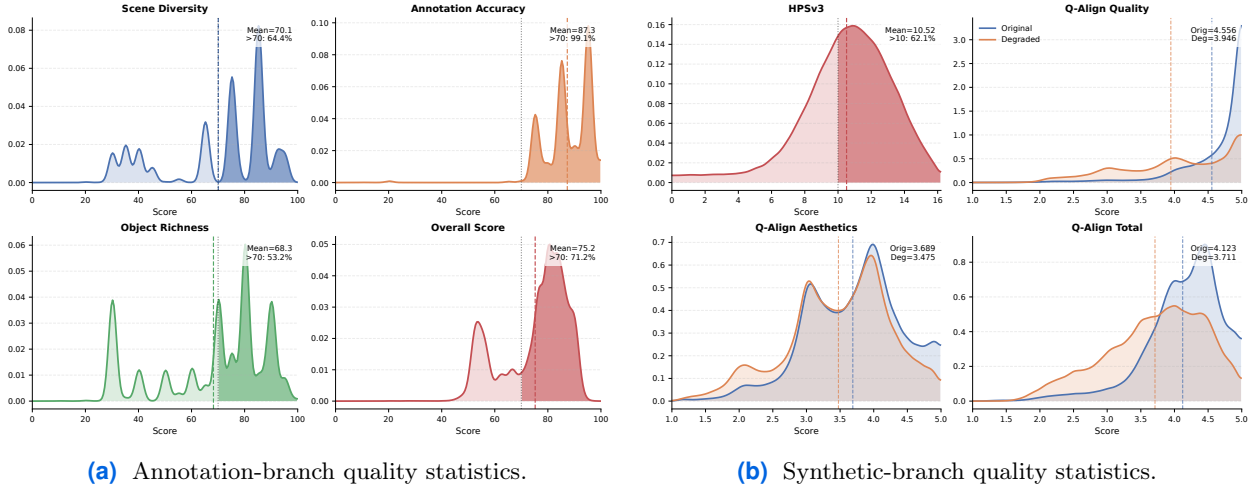


Figure 4 Branch-level filtering statistics used in data curation. Left: after structural correction and validation, the final overall-threshold rule retains 202,750 scene-centric samples from the 750,000-image source pool. Right: among 160,269 valid HPSv3 evaluations, 99,455 exceed the HPSv3 > 10 threshold, and the retained synthetic branch further yields 81,202 edited images and 97,683 refinement pairs after task-specific filtering.

(c) Adaptive Dense Routing. For each demonstration, we assemble a latent prototype bank $B^{(i)} = [z^{(i)}, c_{in}^{(i)}, c_{out}^{(i)}, C^{(i)}]$, applying affine calibration to normalize distinct spaces into a unified bank B_{cal} . Backbone states query this bank via dense cosine routing, where temperature τ is dynamically inferred from $z_{pool} = \text{Mean}(Z)$:

$$\tau = \tau_{\min} + (\tau_{\max} - \tau_{\min}) \cdot \sigma(\text{MLP}_{\tau}(z_{\text{pool}})), \quad (5)$$

$$\mathcal{A}_{t,s} = \frac{\langle \psi(h_t), \mathcal{B}_s \rangle}{\tau}, \quad C_t = \sum_s \text{softmax}(\mathcal{A}_{t,s}) \cdot \mathcal{B}_s. \quad (6)$$

(d) Element-wise Gating Injection. We concatenate normalized backbone hidden states and context C_t to form $X_{\text{gate}} = [\text{LayerNorm}(H_{in,t}); C_t]$. The gating multiplier m_t is computed by a bottleneck MLP: $m_t = \sigma(W_2 \text{GELU}(W_1 X_{\text{gate}} + b_1) + b_2)$. To preserve pre-trained generative priors, W_2 is zero-initialized and b_2 is a positive constant, ensuring m_t starts near identity. Contextual injection is applied multiplicatively as $Y' = Y \odot m_t$, where Y is the SDPA output [30]. This safely modulates attention activations without disrupting established internal representations.

4 Experiments

4.1 Baselines.

We select BAGEL [7] as our primary baseline. Beyond delivering competitive unified understanding and generation performance, BAGEL’s Mixture-of-Transformers architecture enables bidirectional self-attention across the understanding and generation token spaces, thereby allowing CAPM to operate on both branches simultaneously. We compare against two groups. The first is state-of-the-art (SOTA) unified models: UniWorld-V1 [23], Nexus-Gen-V2 [48], and Ovis-U1 [41]. The second is strong open-source MLLMs at various parameter scales: Qwen3-VL [3], Qwen2.5-VL [39], and InternVL-3.5 [42]. We include MLLMs because recent unified models have begun matching them on static understanding benchmarks, making ICL a sharper and more diagnostic test of genuine generalization capability.

4.2 Training Strategy

To stabilize optimization and disentangle understanding and generation dynamics, we employ a two-stage training paradigm on a single H20 GPU node. Both stages use a maximum learning rate of 2×10^{-5} with

Table 3 Composition of UniICL-Bench. The evaluation suite comprises 1,250 curated episodes spanning six cognitive levels and 15 subtasks. All entries marked as MLLM-Judge use Qwen3-VL-30B-A3B-Instruct.

Taxonomy	Sub-task	Modality	Evaluation Metrics	Episodes
Perception	Visual Grounding	Und.	mIoU	100
	Attribute Recognition	Und.	Accuracy	100
	Image Manipulation	Gen.	MLLM-Judge	50
Imitation	Style-Aware Caption	Und.	MLLM-Judge / BERTScore	100
	Scene Reasoning	Und.	MLLM-Judge / BERTScore	100
	Instructional Generation	Gen.	HPSv3	50
Conception	Fast Concept Mapping	Und.	Accuracy	100
	Fast Concept Generation	Gen.	MLLM-Judge	100
Deduction	World-Aware Planning	Und.	Accuracy	100
	Chain-of-Editing	Gen.	MLLM-Judge	50
Analogy	Analogical Inference	Und.	MLLM-Judge	100
	Analogical Editing	Gen.	MLLM-Judge / DINOv3	50
Discernment	Aesthetic Assessment	Und.	SRCC / PLCC	100
	Forgery Detection	Und.	Accuracy	100
	Visual Refinement	Gen.	Q-Align Eff.	50

a 500-step linear warm-up, followed by a constant schedule. **Stage-I: Understanding Warm-up.** We first establish robust In-context adaptation by optimizing solely the understanding ICL objective for 10,000 steps (maximum sequence length of 20,480 tokens) while freezing the generation head. **Stage-II: Unified ICL Training.** Shifting the primary focus to generation ICL, we interleave a small proportion of understanding data to mitigate catastrophic forgetting. The overall loss combines CE and MSE with a 1:1 fixed ratio. This stage trains for 10,000 steps with an expanded 28,672-token maximum sequence length.

4.3 Main Results on UniICL-Bench.

Tab. 4 and Fig. 6 reveal our method achieves the most balanced unified profile, attaining the highest peak understanding and ICL efficiency (78.9/16.9) and leading generation efficiency among unified models. To capture cumulative gains (or degradations) relative to the zero-shot baseline across shot settings, we define ICL efficiency as the normalized area of the performance delta under the k -shot curve:

$$\text{Eff.} = \frac{1}{K_{max}} \sum_{i=1}^n \frac{(P_{k_i} - P_0) + (P_{k_{i-1}} - P_0)}{2} (k_i - k_{i-1}), \quad (7)$$

where $k_i \in \{0, 1, 2, 4, 8\}$, $K_{max} = 8$, and P_0 is the zero-shot performance. These gains stem from robust adaptation across the entire cognitive taxonomy. Profound improvements emerge in complex categories like Conception and Analogy, where our model rapidly adapts within the first two demonstrations while baselines prematurely plateau. By extracting implicit transformation rules rather than relying on sheer model scale, our approach matches or surpasses leading specialized understanding-only MLLMs. Furthermore, our method mitigates the aforementioned *non-monotonic shot scaling* phenomenon. On lower-level tasks with sufficient zero-shot priors, additional context typically introduces cross-modal noise that severely degrades baseline performance. In contrast, our model remains remarkably stable, preserving its zero-shot foundation while capturing gains from informative examples. Conversely, on tasks lacking inherent zero-shot capabilities (e.g., Visual Refinement), our approach leverages few-shot contexts to drive monotonic performance growth. Nevertheless, shot-scaling on fine-grained *Image Manipulation* remains vulnerable as explosive visual contexts overwhelm cross-modal alignment capacities. This foundational perceptual failure directly limits *Analogical Editing* (Fig. 9). Although benefiting from early demonstrations, its higher-shot performance degrades because dense contexts impair image reconstruction. Resolving these scaling bottlenecks remains an open challenge.

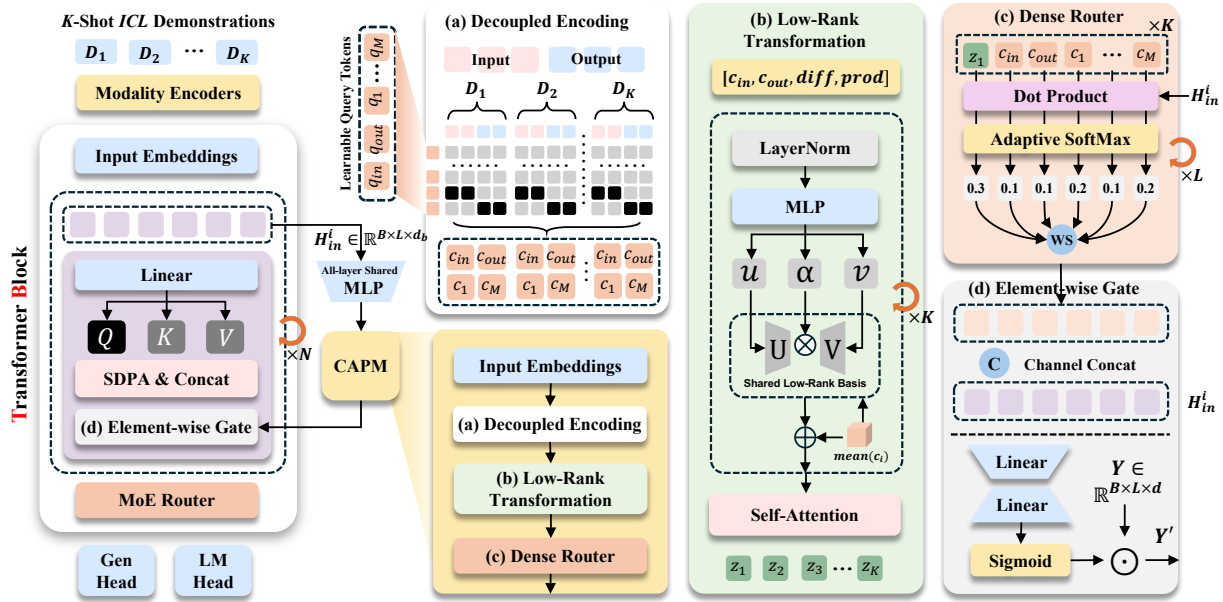


Figure 5 Our lightweight and plug-and-play **CAPM** module adapts to existing Transformer-based models via a four-stage pipeline.

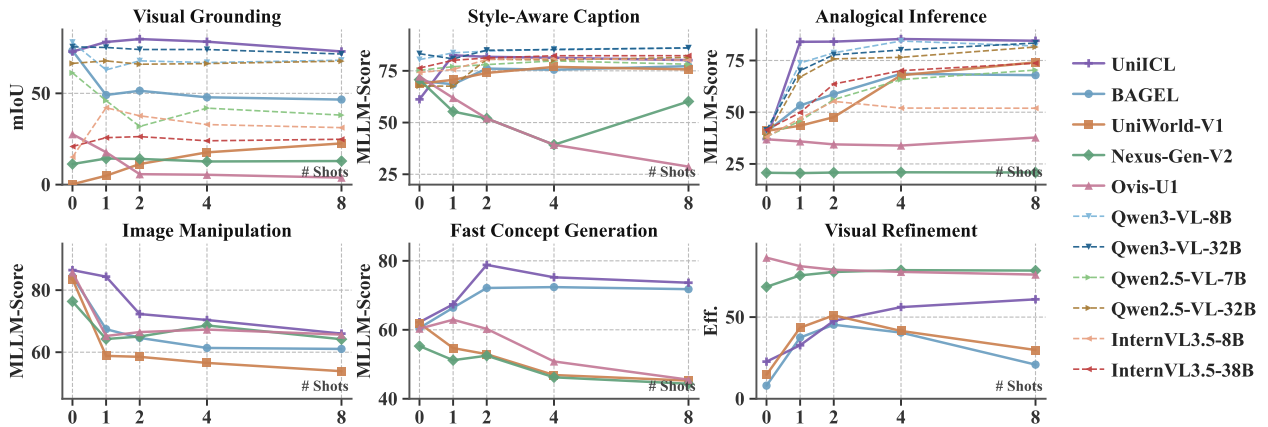


Figure 6 k-shot performance curves for a subset of tasks.

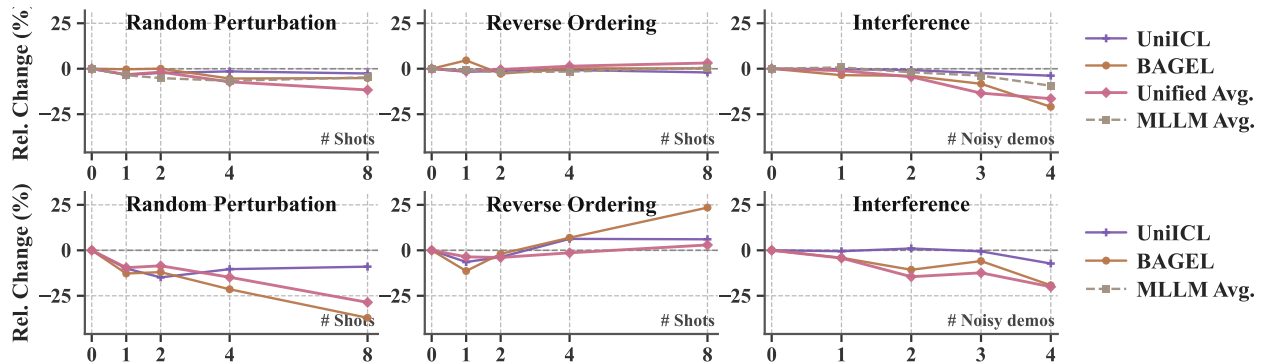


Figure 7 Stability under context perturbations. Top row: understanding. Bottom row: generation. From left to right: random replacement, reverse ordering, and interference with increasing noisy demonstrations.

Table 4 Aggregated main results across the six capability categories. For each category, **Und.** averages understanding-side primary metrics and **Gen.** reports the category’s generation-side metric. Each model is summarized by **Z.s.** (zero-shot), **Pk.** (peak over 0/1/2/4/8-shot), and **Eff.** (ICL efficiency). Z.s./Pk. are on a normalized 0–100 scale.

Model	Stat.	Perception		Imitation		Concept.		Deduction		Analogy		Discern.		Average	
		Und.	Gen.												
Unified Models															
BAGEL	Z.s.	72.7	84.4	69.3	77.0	23.0	60.5	60.0	53.8	40.6	65.3	51.6	8.1	52.8	58.2
	Pk.	72.7	84.4	72.8	77.0	41.0	72.4	60.0	53.8	68.6	65.3	66.4	45.3	59.3	60.5
	Eff.	-14.9	-20.3	2.2	-6.6	11.9	10.8	–	–	22.3	-15.4	6.7	26.1	4.3	-0.3
UniICL (Ours)	Z.s.	66.9	86.5	60.8	78.8	20.0	62.2	88.0	62.2	37.0	68.0	83.1	22.7	59.3	63.4
			↑2.0		↑1.8		↑1.7	↑28.0	↑8.4		↑2.7	↑31.5	↑14.7	↑6.5	↑5.2
	Pk.	80.9	86.5	76.6	79.3	70.0	78.8	88.0	62.2	85.4	74.1	87.3	60.9	78.9	69.6
		↑8.2	↑2.0	↑3.8	↑2.3	↑29.0	↑6.4	↑28.0	↑8.4	↑16.8	↑8.8	↑20.9	↑15.6	↑19.7	↑9.2
	Eff.	9.7	-14.1	13.9	-0.2	39.8	11.5	–	–	44.7	-1.7	3.1	28.0	16.9	4.9
		↑24.6	↑6.3	↑11.6	↑6.4	↑27.9	↑0.7			↑22.4	↑13.8		↑1.9	↑12.5	↑5.2
UniWorld-V1	Z.s.	31.1	83.5	69.4	71.4	23.0	61.9	69.0	53.1	41.0	58.6	55.3	14.7	48.1	57.2
	Pk.	38.8	83.5	73.9	76.2	43.0	61.9	69.0	53.1	74.1	58.6	55.3	51.1	53.9	57.2
	Eff.	2.9	-25.3	3.6	2.8	7.8	-12.3	–	–	19.9	-12.1	-8.2	24.3	1.3	-3.8
Nexus-Gen-V2	Z.s.	39.1	76.4	71.3	57.1	24.0	55.3	51.0	52.5	20.7	67.1	47.6	68.5	42.3	62.8
	Pk.	39.1	76.4	71.3	60.8	33.0	55.3	51.0	52.5	21.0	67.1	63.3	78.7	42.3	62.8
	Eff.	-8.8	-9.6	-11.1	0.9	5.7	-7.2	–	–	0.1	-11.6	10.4	8.9	-2.4	-1.8
Ovis-U1	Z.s.	54.8	85.7	72.1	68.9	22.0	60.3	36.0	58.2	36.9	57.3	62.7	86.4	47.4	69.5
	Pk.	54.8	85.7	72.1	68.9	31.0	62.9	36.0	58.2	37.8	57.3	62.7	86.4	47.4	69.5
	Eff.	-37.2	-18.1	-20.9	-0.4	4.4	-7.0	–	–	-1.5	-4.4	-21.5	-7.9	-13.2	-5.5
MLLMs															
Qwen3-VL-8B	Z.s.	80.5	–	79.5	–	24.0	–	83.0	–	40.9	–	57.6	–	60.9	–
	Pk.	80.5	–	81.6	–	66.0	–	83.0	–	84.4	–	69.4	–	73.5	–
	Eff.	-4.8	–	1.3	–	28.9	–	–	–	37.7	–	5.1	–	9.5	–
Qwen3-VL-32B	Z.s.	79.7	–	83.8	–	24.0	–	82.0	–	41.3	–	68.8	–	63.3	–
	Pk.	80.1	–	85.1	–	63.0	–	82.0	–	83.4	–	68.8	–	75.6	–
	Eff.	0.2	–	0.4	–	18.9	–	–	–	35.5	–	-2.5	–	7.0	–
Qwen2.5-VL-7B	Z.s.	68.1	–	74.7	–	22.0	–	63.0	–	38.2	–	45.6	–	51.9	–
	Pk.	68.1	–	76.1	–	38.0	–	63.0	–	70.4	–	45.6	–	53.5	–
	Eff.	-12.5	–	1.0	–	9.1	–	–	–	22.7	–	-8.6	–	0.3	–
Qwen2.5-VL-32B	Z.s.	72.2	–	72.9	–	24.0	–	68.0	–	38.2	–	65.8	–	56.8	–
	Pk.	72.2	–	79.2	–	38.0	–	68.0	–	81.5	–	71.7	–	68.5	–
	Eff.	-0.7	–	4.6	–	5.5	–	–	–	35.8	–	-5.1	–	6.0	–
InternVL3.5-8B	Z.s.	41.0	–	74.7	–	21.0	–	80.0	–	38.0	–	38.5	–	48.9	–
	Pk.	54.1	–	76.8	–	24.0	–	80.0	–	55.2	–	47.0	–	49.5	–
	Eff.	9.5	–	0.9	–	0.7	–	–	–	13.0	–	-3.4	–	-1.7	–
InternVL3.5-38B	Z.s.	48.4	–	77.9	–	22.0	–	77.0	–	41.5	–	42.0	–	51.5	–
	Pk.	50.0	–	79.2	–	27.0	–	77.0	–	73.7	–	64.1	–	58.7	–
	Eff.	1.1	–	0.7	–	3.4	–	–	–	24.0	–	15.3	–	4.1	–

Table 5 Comparison of ICL Stability: Score represents the area of the deviation region; smaller values indicate better robustness.

Model	Random Replace		Reverse Order		Interference		Average	
	Und.	Gen.	Und.	Gen.	Und.	Gen.	Und.	Gen.
MLLM Avg.	7.3%	–	1.8%	–	6.3%	–	5.1%	–
Unified Avg.	17.2%	15.7%	8.5%	5.7%	11.3%	10.4%	12.4%	10.6%
BAGEL	7.1%	22.0%	2.8%	10.9%	7.9%	7.8%	5.9%	13.6%
Ours	2.1%	10.3%	1.4%	6.1%	1.6%	3.4%	1.7%	6.6%

4.4 Stability Analysis.

Fig. 7 reports results under three perturbation families: interference, random replacement, and reverse ordering. Our method is the most stable across all three, exhibiting the smallest overall degradation; this

Query Input	Reference	Ours	BAGEL	Nexus-Gen-V2	Ovis-U1	UniWorld-V1
Generate a Ana-boot walking past rows of lavender in bloom, Provence-style landscape, midsummer sun (Ana-boot is a duck wearing rain boots)						
Based on your critical assessment, perfect it into a technically flawless and aesthetically superior masterpiece						
The implicit Intent is transformation from a daytime scene to a rainy evening						
Elegant curated sanctuary: twin floral art with "Your Only Limit is you", gold-gray-earth textured sofa, soft warm lighting, muted gradient background, cinematic intimate mood.						
Change the building's stone facade to a vibrant red brick texture while keeping the architectural details and clock visible.						

Figure 8 Qualitative comparison of generative ICL tasks. From top to bottom, we present Fast Concept Generation, Visual Refinement, Analogical Editing, Instructional Generation, and Image Manipulation.

trend is further supported by the forward-feature control study in Fig. 11. Under interference, performance drops progressively as mismatched demonstrations increase, yet our model degrades far more slowly. Random replacement confirms the value of our assembly strategy, as substituting matched demonstrations with random ones consistently hurts performance. Conversely, reverse ordering yields only marginal changes across all models, suggesting ICL relies more on demonstration content than sequence structure. Taken together, performance gains stem from assembling compatible demonstrations rather than their specific presentation order. We also observe a consistent cross-modal asymmetry: generation is substantially more sensitive to demonstration quality than understanding, with markedly larger degradation under interference and random replacement. This suggests generative tasks impose stricter compatibility requirements, as constructing coherent outputs requires more precise contextual grounding than discriminative inference.

4.5 Qualitative Analysis.

Fig. 8 qualitatively compares generation outputs on UniICL-Bench. In few-shot editing scenarios, baselines either fail to capture underlying transformation rules or suffer severe object distortion due to cross-modal interference in longer contexts. Conversely, UniICL extracts implicit structural edits from demonstrations and applies them to the target query, preserving original layouts and visual quality. Figure 10 further shows the benchmark-only *Chain-of-Editing* setting, where the challenge is to maintain step-wise consistency while following a logically progressive edit trajectory rather than simply imitating isolated examples. Together, these visualizations corroborate the quantitative gains in the Analogy and Deduction taxonomy levels.



Figure 9 Failure case on multi-shot image manipulation. UniICL understands task intent but struggles with spatial grounding when multiple transformations overlap in long contexts.

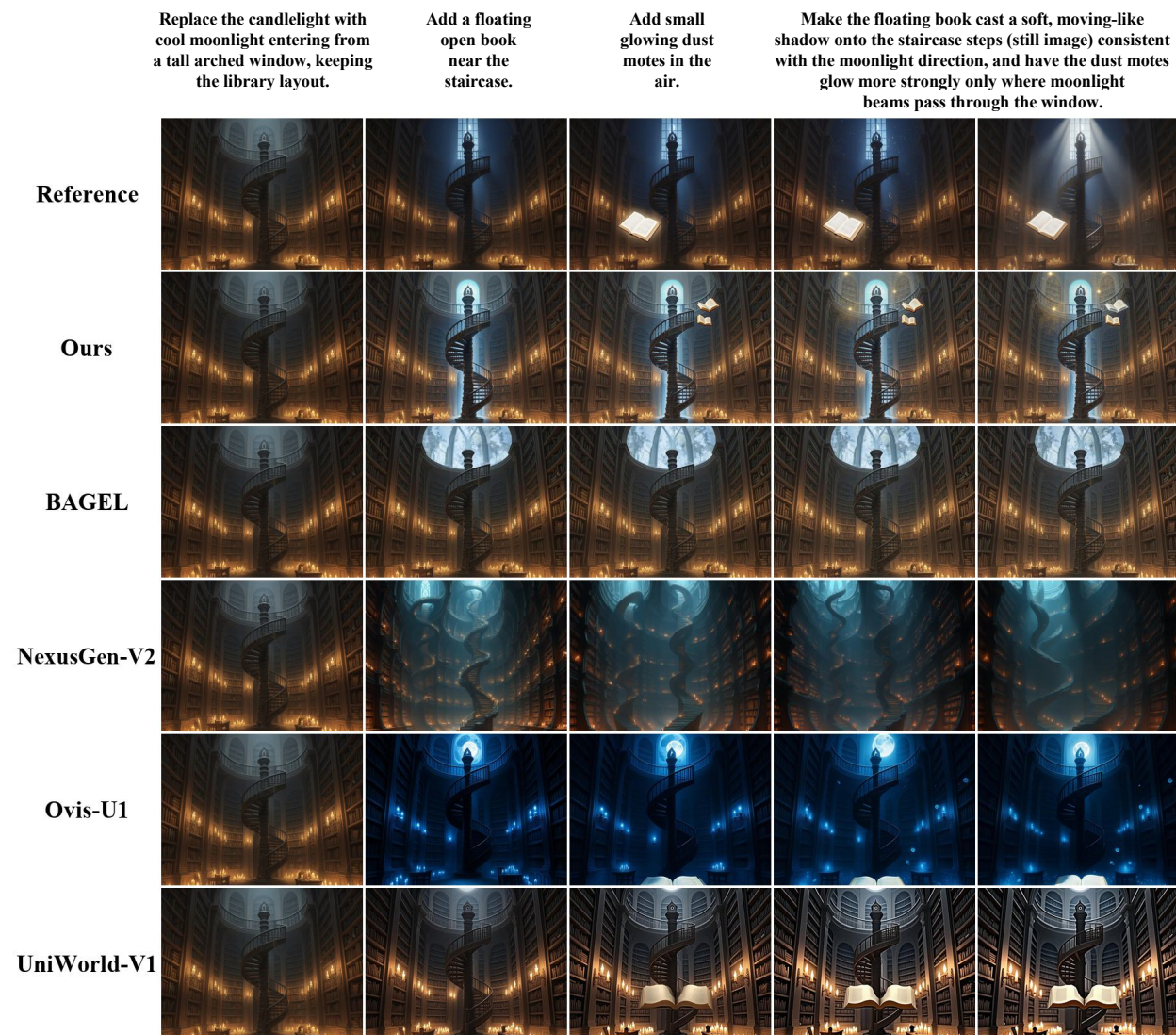


Figure 10 Qualitative comparison on *Chain-of-Editing*. The examples highlight whether the model can follow the demonstrated multi-step editing trajectory while preserving step-wise consistency and image quality.

Table 7 Ablation studies of CAPM module.

(a) CAPM components effect.					(b) CAPM injection depth.				
Setting	Und. Avg.	ICL Eff.	Gen. Avg.	ICL Eff.	Inj. Layers	Und. Avg.	ICL Eff.	Gen. Avg.	ICL Eff.
Ours	78.9	16.9	69.6	4.9	28	78.9	16.9	69.6	4.9
Gate-only	76.2	13.3	66.7	1.2	14	76.3	13.1	69.0	3.4
BAGEL (trained)	75.9	11.2	65.4	0.5	7	76.1	14.4	70.3	3.7
BAGEL	59.3	4.3	60.5	-0.3	0	77.0	15.1	68.6	0.4

Table 8 Branch Transfer ablation: average relative change (%) across shot levels per capability category, compared to the BAGEL baseline. **Gen→Und.**: a Gen-only variant evaluated on understanding tasks; **Und→Gen.**: an Und-only variant evaluated on generation tasks.

Setting	Perception	Imitation	Concept.	Deduction	Analogy	Discern.	Average
Gen→Und.	+7.7%	+0.8%	-7.9%	+1.7%	-0.6%	+11.0%	+2.1%
Und→Gen.	-2.5%	-1.4%	+2.7%	-0.5%	+3.3%	+19.8%	+3.6%

4.6 Human Study.

To complement the qualitative comparison, we conduct a human study on the full generation-side benchmark.

We compare UniICL against Nexus-Gen-V2 over all 350 generation episodes, using the 2-shot protocol for the standard few-shot tasks and the native full-chain setting for *Chain-of-Editing*. As shown in [Tab. 6](#), UniICL achieves a 61.3% overall win rate, with its strongest margin on semantic intent at 64.7%. The preference pattern closely matches the automatic ranking and is consistent with the visual trends in [Figs. 8](#) and [10](#).

Table 6 Human study results.

Metric	Win	Tie	Lose
Semantic Intent	64.7	22.0	13.3
Image Quality	58.0	31.3	10.7
Aesthetics	61.3	26.7	12.0
Overall	61.3	26.7	12.0

4.7 Ablation Studies.

(1) Effect of CAPM Components. We compare four settings: full CAPM (Ours), Gate-only, BAGEL (trained), and the original BAGEL baseline. [Tab. 7-\(a\)](#) shows both trained variants significantly outperform the original baseline, indicating data-driven unified ICL training drives the dominant gain. CAPM provides further improvements over this trained baseline: Ours performs best, while Gate-only slightly exceeds BAGEL (trained). **(2) Impact of Injection Depth.** We vary injection depth from 0/7/14 to full 28-layer insertion. [Tab. 7-\(b\)](#) shows 28-layer injection remains the best balanced configuration. For generation, 7/14-layer injection improves over the 0-layer setting, particularly in ICL efficiency; for understanding, 0/7/14-layer results are close and mildly non-monotonic. Compared to [Tab. 7-\(a\)](#), the 0-layer result still outperforms BAGEL (trained). This suggests CAPM-based training introduces stabilizing regularization even without inference injection, although explicit multi-layer modulation remains necessary for peak performance. **(3) Mutual Impact Between Understanding and Generation.** We compare unified training against single-branch objectives. [Tab. 8](#) indicates complementary effects: Gen-only training improves understanding-side Perception and Discernment but degrades Conception, whereas Und-only training compensates for this deficit on the generation side alongside strong Discernment gains. Discernment uniquely improves in both transfer directions, suggesting it relies on combining perceptual understanding and generative refinement signals. Because one branch’s deficit aligns with the other’s surplus, joint training proves essential for balanced capability development.

Table 9 Alignment between primary and auxiliary metrics across the reported main-experiment model and shot combinations. Pearson and Spearman are computed over all available values in the main results sheet. The *Analogical Editing* row is computed on the unified models only, since understanding-only MLLMs do not produce editing outputs.

Task	Primary	Auxiliary	n	Pearson r	Spearman ρ
Style-Aware Caption	MLLM-Judge	BERTScore	50	0.687	0.612
Scene Reasoning	MLLM-Judge	BERTScore	50	0.116	-0.016
Analogical Editing	MLLM-Judge	DINOv3	25	0.738	0.746
Aesthetic Assessment	SRCC	PLCC	50	0.940	0.914

4.8 Primary and Auxiliary Metrics.

For semantically open-ended tasks, we use MLLM-Judge as the primary metric and report traditional metrics only as auxiliary references. Table 9 quantifies this relationship over all reported model and shot combinations. The alignment is task-dependent rather than universal. For *Style-Aware Caption*, BERTScore follows the judge signal reasonably well, so it is a useful secondary check when correctness depends on both semantic faithfulness and stylistic wording. For *Scene Reasoning*, however, the alignment is weak, indicating that token-overlap metrics are not reliable for ranking open-ended reasoning quality when semantically correct answers differ in surface form. For *Analogical Editing*, DINOv3 similarity and the judge metric move in broadly similar directions, which makes DINOv3 useful as a structural diagnostic. The mismatch cases occur when an edited image stays close in feature space to a plausible target image but misses the intended semantic transformation or under-specifies the requested change. Contrastly, *Aesthetic Assessment* is a scalar ranking problem, so SRCC and PLCC remain highly aligned and either metric provides a stable view of relative model quality.

4.9 Inference Cost of CAPM.

We measure inference cost on the grounding task using the same CAPM-trained checkpoint while varying active injection depth $N \in \{0, 7, 14, 28\}$, where $N=0$ disables CAPM at inference. As shown in Tab. 10, practical inference cost is dominated by shot count rather than CAPM depth. Total latency rises from 1.48–1.54s at 0-shot to 9.47–9.50s at 8-shot, while prefill grows from about 0.53s to 6.94s. At a fixed shot, changing N causes only minor variation, with no monotonic trend as depth increases. Peak VRAM is numerically identical across $N \in \{0, 7, 14, 28\}$ and grows only with longer In-context inputs, from 28,983 MB at 0-shot to 32,211 MB at 8-shot. These results indicate that CAPM adds negligible latency or memory overhead in practice.

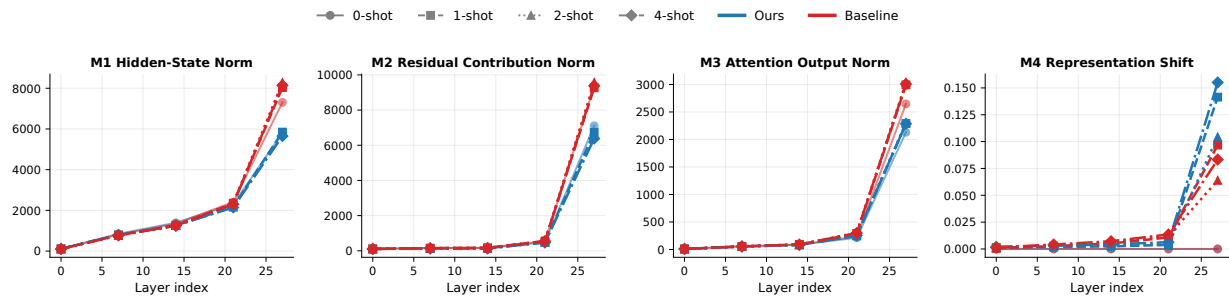
Table 10 Inference cost comparison.

(a) Prefill (ms).						(b) Total (ms).					
N	$K=0$	$K=1$	$K=2$	$K=4$	$K=8$	N	$K=0$	$K=1$	$K=2$	$K=4$	$K=8$
0	535	1154	1778	3285	6943	0	1527	2229	3054	5010	9500
7	534	1156	1777	3281	6936	7	1507	2238	3057	5002	9490
14	532	1152	1773	3274	6925	14	1477	2218	3036	4980	9471
28	535	1155	1778	3281	6941	28	1536	2239	3060	5005	9498

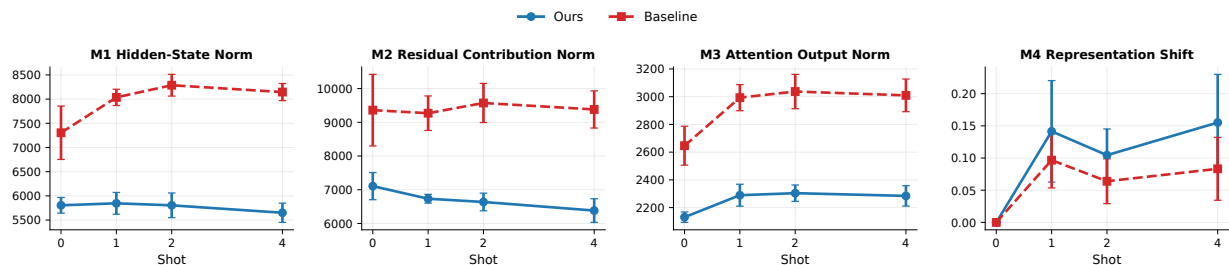
(c) Peak VRAM (MB).				
$K=0$	$K=1$	$K=2$	$K=4$	$K=8$
28,983	29,410	29,794	30,621	32,211

4.10 Control Study on Forward Features.

To probe how CAPM changes few-shot behavior internally, we analyze forward hidden-state statistics on five grounding cases under matched settings, comparing BAGEL and UniICL. Figure 11 tracks four quantities across layers: hidden-state norm, residual contribution norm, attention-output norm, and representation shift to the 0-shot state. At the final layer, UniICL yields consistently larger few-shot representation shifts while keeping late-layer norm growth lower than the baseline. At one, two, and four shots, the final-layer representation shift reaches $1.46\times$, $1.63\times$, and $1.86\times$ that of BAGEL, while hidden-state, residual, and attention-output norms remain lower. The separation between the two models is small in early layers and becomes pronounced only in later layers, suggesting that CAPM mainly acts as targeted late-layer conditioning rather than indiscriminate activation inflation.



(a) Layer-wise trajectories across shots.



(b) Shot sensitivity at the final layer.

Figure 11 Forward-feature control study on five grounding cases. Top: layer-wise behavior under zero, one, two, and four shots. Bottom: shot-wise summary at the final layer. UniICL exhibits larger few-shot representation shift while keeping late-layer norm growth lower than the baseline, indicating more targeted context conditioning rather than activation inflation.

5 Conclusion

We introduce UniICL, a paradigm for training-free adaptation in multimodal understanding and generation. To address few-shot fragility, we propose a six-level Capability-Oriented Taxonomy and construct the UniICL-760K and UniICL-Bench. Our analysis reveals non-monotonic scaling: demonstrations can hinder perception via interference or enhance reasoning through inductive structure. To stabilize this, we propose the Context-Adaptive Prototype Modulator to disentangle context and modulate backbone activations. Results show SOTA performance across unified baselines and competitiveness with specialized models.

Limitation and future work. Reliance on automated synthesis/external models may introduce biases and affect reproducibility. The framework is limited to image-text modalities and short-context regimes. Future work should be extended to video and audio, improve annotation robustness, and explore the interaction between few-shot stability and long-context retrieval across broader domains.

References

- [1] Jean-Baptiste Alayrac, Jeff Donahue, Pauline Luc, Antoine Miech, Iain Barr, Yana Hasson, Karel Lenc, Arthur Mensch, Katherine Millican, Malcolm Reynolds, et al. Flamingo: a visual language model for few-shot learning. *NeurIPS*, 2022. 1, 3, 5
- [2] Anas Awadalla, Irena Gao, Josh Gardner, Jack Hessel, Yusuf Hanafy, Wanrong Zhu, Kalyani Marathe, Yonatan Bitton, Samir Gadre, Shiori Sagawa, et al. Openflamingo: An open-source framework for training large autoregressive vision-language models. *arXiv preprint arXiv:2308.01390*, 2023. 5
- [3] Shuai Bai, Yuxuan Cai, Ruizhe Chen, Keqin Chen, Xionghui Chen, Zesen Cheng, Lianghao Deng, Wei Ding, Chang Gao, Chunjiang Ge, et al. Qwen3-vl technical report. *arXiv preprint arXiv:2511.21631*, 2025. 5, 9
- [4] Tom Brown, Benjamin Mann, Nick Ryder, Melanie Subbiah, Jared D Kaplan, Prafulla Dhariwal, Arvind

- Neelakantan, Pranav Shyam, Girish Sastry, Amanda Askell, et al. Language models are few-shot learners. *NeurIPS*, 2020. 1, 3
- [5] Shuo Chen, Zhen Han, Bailan He, Jianzhe Liu, Mark Buckley, Yao Qin, Philip Torr, Volker Tresp, and Jindong Gu. Can multimodal large language models truly perform multimodal in-context learning? In *2025 IEEE/CVF Winter Conference on Applications of Computer Vision (WACV)*, pages 6000–6010. IEEE, 2025. 1
- [6] Fergus IM Craik and Robert S Lockhart. Levels of processing: A framework for memory research. *Journal of verbal learning and verbal behavior*, 1972. 2, 4
- [7] Chaorui Deng, Deyao Zhu, Kunchang Li, Chenhui Gou, Feng Li, Zeyu Wang, Shu Zhong, Weihao Yu, Xiaonan Nie, Ziang Song, et al. Emerging properties in unified multimodal pretraining. *arXiv preprint arXiv:2505.14683*, 2025. 3, 9
- [8] Runpei Dong, Chunrui Han, Yuang Peng, Zekun Qi, Zheng Ge, Jinrong Yang, Liang Zhao, Jianjian Sun, Hongyu Zhou, Haoran Wei, et al. Dreamllm: Synergistic multimodal comprehension and creation. *arXiv preprint arXiv:2309.11499*, 2023. 1, 3
- [9] Daniel J Felleman and David C Van Essen. Distributed hierarchical processing in the primate cerebral cortex. *Cerebral cortex (New York, NY: 1991)*, 1991. 2, 4
- [10] Dhruva Ghosh, Hannaneh Hajishirzi, and Ludwig Schmidt. Geneval: An object-focused framework for evaluating text-to-image alignment. *Advances in Neural Information Processing Systems*, 2023. 6, 8
- [11] Graeme S Halford, William H Wilson, and Steven Phillips. Processing capacity defined by relational complexity: Implications for comparative, developmental, and cognitive psychology. *Behavioral and brain sciences*, 1998. 2, 4
- [12] Jack Hessel, Ari Holtzman, Maxwell Forbes, Ronan Le Bras, and Yejin Choi. Clipscore: A reference-free evaluation metric for image captioning. In *EMNLP*, 2021. 7
- [13] Wenyi Hong, Wenmeng Yu, Xiaotao Gu, Guo Wang, Guobing Gan, Haomiao Tang, Jiale Cheng, Ji Qi, Junhui Ji, Lihang Pan, et al. Glm-4.5 v and glm-4.1 v-thinking: Towards versatile multimodal reasoning with scalable reinforcement learning. *arXiv preprint arXiv:2507.01006*, 2025. 5
- [14] Qing Jiang, Junan Huo, Xingyu Chen, Yuda Xiong, Zhaoyang Zeng, Yihao Chen, Tianhe Ren, Junzhi Yu, and Lei Zhang. Detect anything via next point prediction, 2025. URL <https://arxiv.org/abs/2510.12798>. 5
- [15] Jing Yu Koh, Daniel Fried, and Russ R Salakhutdinov. Generating images with multimodal language models. *NeurIPS*, 2023. 1, 3
- [16] Hugo Laurençon, Léo Tronchon, Matthieu Cord, and Victor Sanh. What matters when building vision-language models? *NeurIPS*, 2024. 3
- [17] Bo Li, Yuanhan Zhang, Liangyu Chen, Jinghao Wang, Fanyi Pu, Jingkang Yang, Chunyuan Li, and Ziwei Liu. Mimic-it: Multi-modal in-context instruction tuning. 2023. 1
- [18] Bo Li, Yuanhan Zhang, Liangyu Chen, Jinghao Wang, Fanyi Pu, Joshua Adrian Cahyono, Jingkang Yang, Chunyuan Li, and Ziwei Liu. Otter: A multi-modal model with in-context instruction tuning. *T-PAMI*, 2025. 1
- [19] Bohao Li, Rui Wang, Guangzhi Wang, Yuying Ge, Yixiao Ge, and Ying Shan. Seed-bench: Benchmarking multimodal llms with generative comprehension. *arXiv preprint arXiv:2307.16125*, 2023. 1, 3, 8
- [20] Junnan Li, Dongxu Li, Silvio Savarese, and Steven Hoi. Blip-2: Bootstrapping language-image pre-training with frozen image encoders and large language models. In *ICML*, 2023. 1, 3
- [21] Yanshu Li, Hongyang He, Yi Cao, Qisen Cheng, Xiang Fu, and Ruixiang Tang. M2iv: Towards efficient and fine-grained multimodal in-context learning in large vision-language models. *arXiv e-prints*, pages arXiv–2504, 2025. 1
- [22] Zhong-Yu Li, Ruoyi Du, Juncheng Yan, Le Zhuo, Zhen Li, Peng Gao, Zhanyu Ma, and Ming-Ming Cheng. Visualcloze: A universal image generation framework via visual in-context learning. In *ICCV*, 2025. 1, 3
- [23] Bin Lin, Zongjian Li, Xinhua Cheng, Yuwei Niu, Yang Ye, Xianyi He, Shenghai Yuan, Wangbo Yu, Shaodong Wang, Yunyang Ge, et al. Uniworld-v1: High-resolution semantic encoders for unified visual understanding and generation. *arXiv preprint arXiv:2506.03147*, 2025. 3, 9
- [24] Yuan Liu, Haodong Duan, Yuanhan Zhang, Bo Li, Songyang Zhang, Wangbo Zhao, Yike Yuan, Jiaqi Wang, Conghui He, Ziwei Liu, et al. Mmbench: Is your multi-modal model an all-around player? In *ECCV*, 2024. 1, 3, 6, 8

- [25] Shayne Longpre, Le Hou, Tu Vu, Albert Webson, Hyung Won Chung, Yi Tay, Denny Zhou, Quoc V Le, Barret Zoph, Jason Wei, et al. The flan collection: Designing data and methods for effective instruction tuning. In *ICML*, 2023. 3
- [26] Yao Lu, Max Bartolo, Alastair Moore, Sebastian Riedel, and Pontus Stenetorp. Fantastically ordered prompts and where to find them: Overcoming few-shot prompt order sensitivity. In *ACL*, 2022. 1
- [27] Yuhang Ma, Xiaoshi Wu, Keqiang Sun, and Hongsheng Li. Hpsv3: Towards wide-spectrum human preference score. In *ICCV*, 2025. 6, 7
- [28] Catherine Olsson, Nelson Elhage, Neel Nanda, Nicholas Joseph, Nova DasSarma, Tom Henighan, Ben Mann, Amanda Askell, Yuntao Bai, Anna Chen, et al. In-context learning and induction heads. *arXiv preprint arXiv:2209.11895*, 2022. 3
- [29] Libo Qin, Qiguang Chen, Hao Fei, Zhi Chen, Min Li, and Wanxiang Che. What factors affect multi-modal in-context learning? an in-depth exploration. *Advances in Neural Information Processing Systems*, 2024. 1
- [30] Zihan Qiu, Zekun Wang, Bo Zheng, Zeyu Huang, Kaiyue Wen, Songlin Yang, Rui Men, Le Yu, Fei Huang, Suozhi Huang, et al. Gated attention for large language models: Non-linearity, sparsity, and attention-sink-free. *arXiv preprint arXiv:2505.06708*, 2025. 9
- [31] Nikhila Ravi, Valentin Gabeur, Yuan-Ting Hu, Ronghang Hu, Chaitanya Ryali, Tengyu Ma, Haitham Khedr, Roman Rädle, Chloe Rolland, Laura Gustafson, et al. Sam 2: Segment anything in images and videos. *arXiv preprint arXiv:2408.00714*, 2024. 5
- [32] Christoph Schuhmann, Romain Beaumont, Richard Vencu, Cade Gordon, Ross Wightman, Mehdi Cherti, Theo Coombes, Aarush Katta, Clayton Mullis, Mitchell Wortsman, et al. Laion-5b: An open large-scale dataset for training next generation image-text models. *NeurIPS*, 2022. 5
- [33] Oriane Siméoni, Huy V Vo, Maximilian Seitzer, Federico Baldassarre, Maxime Oquab, Cijo Jose, Vasil Khalidov, Marc Szafraniec, Seungeun Yi, Michaël Ramamonjisoa, et al. Dinov3. *arXiv preprint arXiv:2508.10104*, 2025. 6
- [34] Quan Sun, Qiyang Yu, Yufeng Cui, Fan Zhang, Xiaosong Zhang, Yueze Wang, Hongcheng Gao, Jingjing Liu, Tiejun Huang, and Xinlong Wang. Emu: Generative pretraining in multimodality. *arXiv preprint arXiv:2307.05222*, 2023. 3
- [35] Quan Sun, Yufeng Cui, Xiaosong Zhang, Fan Zhang, Qiyang Yu, Yueze Wang, Yongming Rao, Jingjing Liu, Tiejun Huang, and Xinlong Wang. Generative multimodal models are in-context learners. In *CVPR*, 2024. 3
- [36] Zineng Tang, Ziyi Yang, Mahmoud Khademi, Yang Liu, Chenguang Zhu, and Mohit Bansal. Codi-2: In-context interleaved and interactive any-to-any generation. In *CVPR*, 2024. 3
- [37] Alex Kulesza Ben Taskar. Determinantal point processes for machine learning. *stat*, 2013. 6
- [38] Chameleon Team. Chameleon: Mixed-modal early-fusion foundation models. *arXiv preprint arXiv:2405.09818*, 2024. 3
- [39] Qwen Team. Qwen2.5-vl, January 2025. URL <https://qwenlm.github.io/blog/qwen2.5-vl/>. 9
- [40] Johannes Von Oswald, Eyvind Niklasson, Ettore Randazzo, João Sacramento, Alexander Mordvintsev, Andrey Zhmoginov, and Max Vladymyrov. Transformers learn in-context by gradient descent. In *ICML*, 2023. 3
- [41] Guo-Hua Wang, Shanshan Zhao, Xinjie Zhang, Liangfu Cao, Pengxin Zhan, Lunhao Duan, Shiyin Lu, Minghao Fu, Xiaohao Chen, Jianshan Zhao, et al. Ovis-u1 technical report. *arXiv preprint arXiv:2506.23044*, 2025. 3, 9
- [42] Weiyun Wang, Zhangwei Gao, Lixin Gu, Hengjun Pu, Long Cui, Xingguang Wei, Zhaoyang Liu, Linglin Jing, Shenglong Ye, Jie Shao, et al. Internvl3. 5: Advancing open-source multimodal models in versatility, reasoning, and efficiency. *arXiv preprint arXiv:2508.18265*, 2025. 9
- [43] Xinlong Wang, Xiaosong Zhang, Zhengxiong Luo, Quan Sun, Yufeng Cui, Jinsheng Wang, Fan Zhang, Yueze Wang, Zhen Li, Qiyang Yu, et al. Emu3: Next-token prediction is all you need. *arXiv preprint arXiv:2409.18869*, 2024. 3
- [44] Yizhong Wang, Swaroop Mishra, Pegah Alipoormolabashi, Yeganeh Kordi, Amirreza Mirzaei, Atharva Naik, Arjun Ashok, Arut Selvan Dhanasekaran, Anjana Arunkumar, David Stap, et al. Super-naturalinstructions: Generalization via declarative instructions on 1600+ nlp tasks. In *EMNLP*, 2022. 3

- [45] Haoning Wu, Zicheng Zhang, Weixia Zhang, Chaofeng Chen, Liang Liao, Chunyi Li, Yixuan Gao, Annan Wang, Erli Zhang, Wenxiu Sun, et al. Q-align: Teaching llms for visual scoring via discrete text-defined levels. *arXiv preprint arXiv:2312.17090*, 2023. [6](#), [7](#)
- [46] Sang Michael Xie, Aditi Raghunathan, Percy Liang, and Tengyu Ma. An explanation of in-context learning as implicit bayesian inference. *arXiv preprint arXiv:2111.02080*, 2021. [3](#)
- [47] Xiang Yue, Yuansheng Ni, Kai Zhang, Tianyu Zheng, Ruoqi Liu, Ge Zhang, Samuel Stevens, Dongfu Jiang, Weiming Ren, Yuxuan Sun, et al. Mmmu: A massive multi-discipline multimodal understanding and reasoning benchmark for expert agi. In *CVPR*, 2024. [1](#), [3](#), [6](#), [8](#)
- [48] Hong Zhang, Zhongjie Duan, Xingjun Wang, Yuze Zhao, Weiyi Lu, Zhipeng Di, Yixuan Xu, Yingda Chen, and Yu Zhang. Nexus-gen: Unified image understanding, generation, and editing via prefilled autoregression in shared embedding space. *arXiv preprint arXiv:2504.21356*, 2025. [3](#), [9](#)
- [49] Yanzhao Zhang, Mingxin Li, Dingkun Long, Xin Zhang, Huan Lin, Baosong Yang, Pengjun Xie, An Yang, Dayiheng Liu, Junyang Lin, et al. Qwen3 embedding: Advancing text embedding and reranking through foundation models. *arXiv preprint arXiv:2506.05176*, 2025. [6](#)
- [50] Youcai Zhang, Xinyu Huang, Jinyu Ma, Zhaoyang Li, Zhaochuan Luo, Yanchun Xie, Yuzhuo Qin, Tong Luo, Yaqian Li, Shilong Liu, et al. Recognize anything: A strong image tagging model. In *CVPR*, 2024. [5](#)
- [51] Haozhe Zhao, Zefan Cai, Shuzheng Si, Xiaojian Ma, Kaikai An, Liang Chen, Zixuan Liu, Sheng Wang, Wenjuan Han, and Baobao Chang. Mmicl: Empowering vision-language model with multi-modal in-context learning. *arXiv preprint arXiv:2309.07915*, 2023. [1](#)
- [52] Lianmin Zheng, Wei-Lin Chiang, Ying Sheng, Siyuan Zhuang, Zhanghao Wu, Yonghao Zhuang, Zi Lin, Zhuohan Li, Dacheng Li, Eric Xing, et al. Judging llm-as-a-judge with mt-bench and chatbot arena. *NeurIPS*, 2023. [7](#)
- [53] Yongshuo Zong, Ondrej Bohdal, and Timothy Hospedales. Vl-icl bench: The devil in the details of multimodal in-context learning. *arXiv preprint arXiv:2403.13164*, 2024. [7](#), [8](#)